Self-consistent molecular dynamics formulation for electric-field-mediated electrolyte transport through nanochannels

A. V. Raghunathan and N. R. Aluru*

*Department of Mechanical Science and Engineering, Beckman Institute for Advanced Science and Technology,
University of Illinois at Urbana-Champaign, Urbana, Illinois 61801, USA*
(Received 2 March 2007; published 17 July 2007)

A self-consistent molecular dynamics (SCMD) formulation is presented for electric-field-mediated transport of water and ions through a nanochannel connected to reservoirs or baths. The SCMD formulation is compared with a uniform field MD approach, where the applied electric field is assumed to be uniform, for 2 nm and 3.5 nm wide nanochannels immersed in a $0.5M$ KCl solution. Reservoir ionic concentrations are maintained using the dual-control-volume grand canonical molecular dynamics technique. Simulation results with varying channel height indicate that the SCMD approach calculates the electrostatic potential in the simulation domain more accurately compared to the uniform field approach, with the deviation in results increasing with the channel height. The translocation times and ionic fluxes predicted by uniform field MD can be substantially different from those predicted by the SCMD approach. Our results also indicate that during a 2 ns simulation time K^+ ions can permeate through a 1 nm channel when the applied electric field is computed self-consistently, while the permeation is not observed when the electric field is assumed to be uniform.

PACS number(s): 66.10.−x, 82.39.Wj, 68.08.−p, 47.11.Mn

I. INTRODUCTION

Understanding the behavior of water and electrolytes in confined geometries such as nanopores and nanometer channels is of significant interest to many applications in biology and engineering [1]. For example, selective transport of ions in biological ion channels is responsible for the generation of action potentials in nerves and muscles and the regulation of hormone release from endocrine cells [2]. Similarly, water and ion transport in engineered and synthetic ion channels is essential to the development of novel sensing, energy, and desalination systems [3]. A popular mechanism to transport water and ions through nanopores and nanochannels is to use an external electric field. Modeling and simulation of electrically mediated fluid flow in nanometer-wide channels and pores can help address many of the fundamental issues governing water and ion transport and enable rapid design of nanofluidic systems [4]. The majority of simulations analyzing the flow of ions through nanochannels have been performed using the Nernst-Planck (NP) [5,6], Poisson-Nernst-Planck (PNP) [7,8], and Brownian dynamics (BD) [9,10] simulations. These methods typically treat ions as point charges and water as a dielectric continuum and, hence, their applicability to accurately simulate confined nanochannels, where the molecular nature of the ions, the discreteness of the water molecules, and the interfacial behavior can significantly affect the transport and dynamical properties [11,12], can be questionable.

Recent developments in molecular dynamics (MD) simulation of biological membranes and artificial nanochannels have made it possible to understand ion and water transport, and selectivity in nanoconfined geometries [13]. Atomistic models of infinitely long nanochannels have been studied in great detail to analyze the structure and diffusion of water molecules inside the channel [14,15]. Nonequilibrium MD studies of membranes with an externally applied field have helped in understanding the transport, dynamical properties, and energetics of ions in nanochannels [16]. To investigate the entry of ions and water into the nanochannel (or nanopore) due to an applied external electric field, a nanochannel (or nanopore) with finite length immersed in a bath was investigated using BD [17] and MD [18] simulations. The external electrical potentials are applied at either end of the bath-nanochannel-bath system (hereafter, simply referred to as the nanochannel-bath system), and a uniform external electric field was assumed to be applied throughout the nanochannel-bath system. This is referred to as the "uniform field" approximation in this paper. Typically, the size of the bath is much larger compared to the critical size (width or diameter) of the nanochannel and assuming a uniform applied electric field in the entire nanochannel-bath system can be a gross simplification. Ramakrishnan *et al.* [19] modified the uniform field approach and applied a higher external electric field inside the nanochannel and a lower electric field in the bath, accounting for the water polarization near the channel wall. In this paper, we introduce a self-consistent MD (SCMD) methodology to accurately account for the applied external electric field in a MD simulation due to immersed electrodes. In Sec. II, we introduce the SCMD formulation. The dual-control-volume grand canonical molecular dynamics technique (DCV-GCMD) that is used to maintain the ion concentration in the bath is described in Sec. III. Section IV provides the simulation details and verification of the DCV-GCMD technique is discussed in Sec. V. Numerical results comparing the electrical potential and field distribution, ionic flux, and transport properties obtained using SCMD, uniform field MD, and continuum theory are presented in Sec. VI. Finally, conclusions are presented in Sec. VII.

---

*Corresponding author. Electronic address: aluru@uiuc.edu;
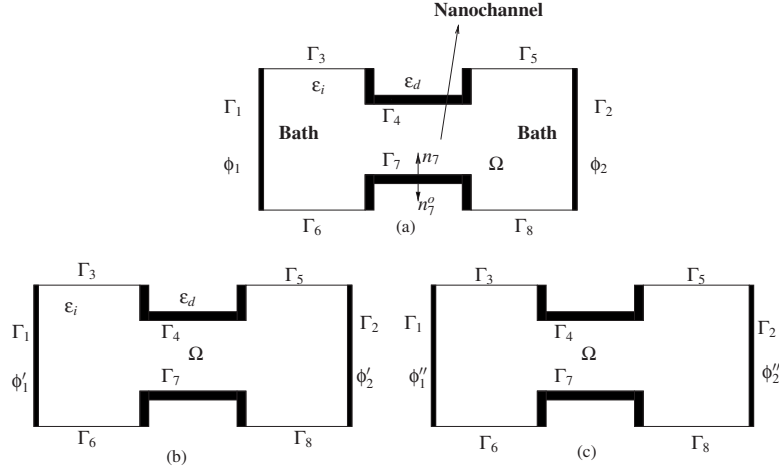URL: http://www.uiuc.edu/~aluru

FIG. 1. The domain and boundaries of (a) the electrostatic problem to be solved [given by Eq. (6)] and its decomposition into (b) the particular solution [given by Eq. (9)] and (c) the homogeneous solution [given by Eq. (12)]. Ω is the entire nanochannel-bath system, Γ's denote the various boundaries, ϵ_i is the dielectric constant of the fluid in contact with the channel wall, and ϵ_d is the dielectric constant of the membrane exterior to the channel wall.

II. SELF-CONSISTENT FORMULATION

A nanochannel-bath system filled with an electrolyte solution is shown in Fig. 1. The Poisson equation, solved in the electrostatic domain Ω (see Fig. 1), for this system is given by:

$$\nabla \cdot (\epsilon_i \nabla \phi) = -\rho_{ions} = -F \sum_{i=1}^{N} z_i c_i \quad \text{in } \Omega, \tag{1}$$

where ϕ is the electrostatic potential, ϵ_i $(=\epsilon_r \epsilon_0)$ is the dielectric permittivity of the fluid medium, ϵ_r is the relative dielectric permittivity, ϵ_0 is the dielectric constant of vacuum, ρ_{ions} is the charge density of the ions, N is the number of ionic species, c_i is the concentration of the ith ionic species, z_i is the valence of ion i, and F is the Faraday's constant.

The externally applied electrostatic potential on the electrodes at Γ_1 and Γ_2 will enforce a Dirichlet boundary condition—i.e.,

$$\phi = \phi_1 \quad \text{on } \Gamma_1, \tag{2}$$

$$\phi = \phi_2 \quad \text{on } \Gamma_2. \tag{3}$$

The boundary conditions on the top and bottom surfaces Γ_3, Γ_5, Γ_6, and Γ_8 of the baths are given by (symmetric boundary conditions)

$$\frac{\partial \phi}{\partial n} = 0 \quad \text{on } \Gamma_j \quad \text{for } j = 3, 5, 6, 8. \tag{4}$$

The boundary conditions on the channel wall interfaces Γ_4 and Γ_7 are

$$\epsilon_i \frac{\partial \phi}{\partial n_j} = \epsilon_d \frac{\partial \phi}{\partial n_j^d} \quad \text{on } \Gamma_j \quad \text{for } j = 4, 7, \tag{5}$$

where n_j and n_j^d denote the inward and outward normals on the boundary Γ_j. ϵ_d is the dielectric constant of the exterior (or outward) medium. Note that in the approach described

below, the values of ϵ_i and ϵ_d are not needed to satisfy this boundary condition.

Due to the "layering" of water molecules in the interfacial region [20], the dielectric constant of water at the interface and inside the nanochannel is typically reduced [21] and cannot be estimated accurately without a molecular description of water. Therefore, in solving for electrostatics in MD, the charge density of water molecules, ρ_{water}, is included explicitly in the Poisson equation—i.e., $\rho_{total} = \rho_{ions} + \rho_{water}$. Assuming a dielectric constant of vacuum ($\epsilon_r = 1$), Eq. (1) becomes

$$\nabla \cdot (\nabla \phi) = -\frac{\rho_{total}}{\epsilon_0} \quad \text{in } \Omega. \tag{6}$$

There are two major issues while trying to solve Eq. (6) directly. First, as water molecules are accounted for in the charge density explicitly, the domain Ω has to be resolved into a fine grid with a grid-size comparable to the radius of a single water molecule (≈ 1 Å). Second, the charge density is assumed to have a continuous distribution which can lead to an error in the calculated electrostatic potential, as the ionic charges are discrete in nature. Both these limitations are resolved by decomposing Eq. (6) into a *particular solution* for the charge distribution in an unbounded domain and a *homogeneous solution* within the given domain, with appropriate boundary conditions [22]. Therefore, the solution to the Poisson problem, ϕ, is now the sum of two solutions:

$$\phi = \phi' + \phi'', \tag{7}$$

$$\frac{\partial \phi}{\partial n} = \frac{\partial \phi'}{\partial n} + \frac{\partial \phi''}{\partial n}, \tag{8}$$

where ϕ' is the particular solution and ϕ'' is the homogeneous solution. The particular solution ϕ' is computed by solving the following equation in the unbounded domain:
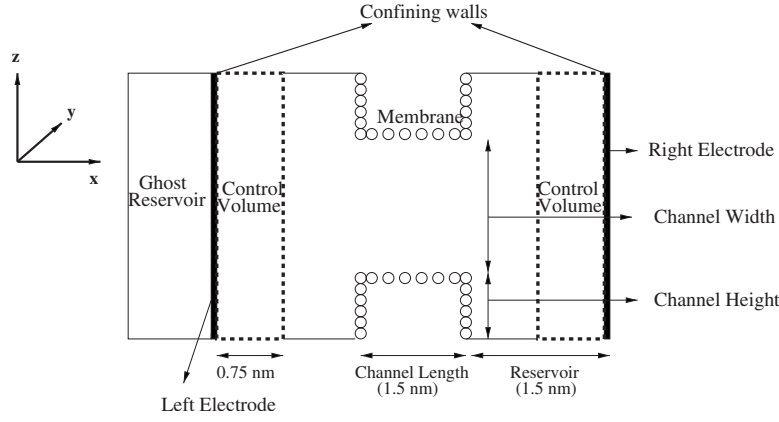
FIG. 2. A sketch of a nanochannel-bath system to investigate electric field-mediated transport. The two control volumes on either side are maintained at a constant chemical potential using DCV-GCMD.

$$\boldsymbol{\nabla} \cdot (\boldsymbol{\nabla}\phi') = -\frac{\rho_{total}}{\epsilon_0} \quad \text{in } \Omega \cup \Omega', \tag{9}$$

where Ω' is the domain exterior to Ω. The solution to Eq. (9) is given by [23]:

$$\phi'(R) = \int_{\Omega \cup \Omega'} \frac{\rho_{total}(r)dv}{4\pi\epsilon_0 |R - r|} \tag{10}$$

$$= \sum_{i=1}^{N_q} \frac{q_i}{4\pi\epsilon_0 |R - r_i|}. \tag{11}$$

Here, R is the point in space where the potential ϕ' is calculated, $\rho_{\text{total}}(r)$ is the charge density at position r, q_i is the charge on the ith atom in the system, N_q is the total number of charged atoms in the system, which includes both ions and water, and r_i is the coordinate of the charged atom i in the system. The particular solution can be obtained by using a direct summation calculation of the Coulomb interactions or by using particle methods for fast summations [24]. In this study, the particle mesh Ewald (PME) [25] method was used with a correction of the Ewald summation given by Yeh and Berkowtz [26] to remove the periodicity in the x direction and calculate ϕ' from Eq. (11). The solution to Eq. (11) gives $\phi' = \phi'_i$ on Γ_i, $i = 1, 2$, and $\frac{\partial\phi'}{\partial n} = \left(\frac{\partial\phi'}{\partial n}\right)_i$ on Γ_i, $i = 3, \dots, 8$.

To obtain the homogeneous solution, appropriate boundary conditions need to be applied such that the decomposed solution retains the same boundary conditions as applied in the original problem. The homogeneous equation along with the corresponding boundary conditions is given by

$$\boldsymbol{\nabla} \cdot (\boldsymbol{\nabla}\phi'') = 0 \quad \text{in } \Omega, \tag{12}$$

$$\phi'' = \phi_1 - \phi' \quad \text{on } \Gamma_1, \tag{13}$$

$$\phi'' = \phi_2 - \phi' \quad \text{on } \Gamma_2, \tag{14}$$

$$\frac{\partial\phi''}{\partial n} = \frac{\partial\phi}{\partial n} - \frac{\partial\phi'}{\partial n} \quad \text{on } \Gamma_i, \ i = 3,5,6,8, \tag{15}$$

$$\frac{\partial\phi''}{\partial n} = 0 \quad \text{on } \Gamma_i, \ i = 4, 7. \tag{16}$$

Since the water and wall dielectric properties are explicitly taken into account in the particular solution, we impose the boundary condition given in Eq. (16) on Γ_4 and Γ_7 for the homogeneous equation. Other boundary conditions (e.g., $\frac{\partial\phi}{\partial n} = 0$) on Γ_4 and Γ_7 can also be easily implemented in the approach presented here.

During each MD time step, Eq. (12) was solved using a finite-difference scheme with a grid size of 0.25 nm. ϕ'' thus obtained was mapped onto the atoms in the system using the linear least-squares method [27]. The self-consistent simulation methodology described above was adapted into the MD simulation software GROMACS [28]. Implementation of the electrostatic potential calculation in MD using this self-consistent decomposition is relatively simple. The use of coarse grids in discretization of Eq. (12) makes this decomposition computationally less expensive as compared to directly solving the Poisson Eq. (6).

III. DUAL-CONTROL-VOLUME GRAND CANONICAL MOLECULAR DYNAMICS

In the nanochannel-bath setup [see Fig. 1(a)], K^+ and Cl^- ions migrate from one bath to the other through the nanochannel in the presence of an external electric field. This causes the depletion or the accumulation of the ions in the bath. The concentration of K^+ and Cl^- ions needs to be maintained constant in the bath. For this purpose, a grand canonical (μVT) MD simulation is needed to maintain the chemical potential (and concentration), volume and temperature in the MD simulation [29–32]. The two baths in the nanochannel-bath setup are considered to be the two control volumes where the concentration needs to be maintained. Using the DCV-GCMD technique proposed by Heffelfinger and van Swol [33], the chemical potential (and concentration) within the control volumes is maintained. The original DCV-GCMD technique was developed for Lennard-Jones (LJ) fluids, and in this study it has been extended to electrolytic solutions. Though the DCV-GCMD technique is necessary for the model investigated here, it is computationally more expen-

sive than standard *NVT* or *NVE* MD simulations due to the extra effort required in the insertion and deletion of particles into the system.

For the DCV-GCMD simulation of the nanochannel-bath system, a control volume is placed in each of the two baths (see Fig. 2). The control volumes are provided with the chemical potential of the ionic species (K^+ and Cl^- ions) that needs to be maintained during the MD simulation. During the simulation, the stochastic insertion or deletion trials are performed every n_{MD} time steps in MD. The MD simulation is "frozen" in time after every n_{MD} time steps. This is followed by a number of stochastic insertion or deletion trials, denoted by n_{trial}, performed in each control volume, using the Metropolis algorithm [34]. This "stochastic" step maintains the chemical potential and concentration of the K^+ and Cl^- ions in the control volume. A "ghost" reservoir containing LJ atoms is attached to the simulation setup (see Fig. 2). The "ghost" reservoir contains LJ atoms with no charge and these atoms do not enter the nanochannel-bath system due to the presence of the confining walls. Whenever an ion is deleted from the control volume, it is placed into the "ghost" reservoir, and if an atom needs to be inserted into the control volume, it is taken from the "ghost" reservoir. This reservoir thus ensures that the total number of atoms in the MD simulation is constant during DCV-GCMD. It should be noted that the "ghost" reservoir is used only to overcome a software limitation and is not critical for the implementation of DCV-GCMD. During the trial insertions or deletions, the change in potential energy, ΔU, for inserting or deleting an ion in the control volume is calculated by summing the electrostatic and LJ interactions. ΔU is used in the insertion or deletion acceptance criteria in DCV-GCMD, as well as to calculate the chemical potential of the control volume using the Widom's particle insertion method [35]. The DCV-GCMD simulation procedure, given in algorithm 1 in the Appendix, has been implemented in GROMACS [28,36].

During the stochastic step, the probability of a trial insertion or deletion (of K^+ or Cl^- ions) in the control volumes is equal. The probability of adjusting the number of any one of the K^+ or Cl^- ions in the control volume is also the same. Trial insertion of an ionic species i into the control volume is accepted if

$$\left[\frac{1}{N_i(c)+1}\right]\exp\left[\beta\mu_i(c)+\ln\frac{V(c)}{\Lambda_i^3}-\beta\Delta U_i\right]\geqslant\xi, \quad (17)$$

where $V(c)$, $N_i(c)$, and $\mu_i(c)$ are the volume, number of ions of type i, and the input chemical potential of type i in the control volume c, respectively. $\beta=1/k_BT$ where k_B is Boltzmann's constant and T is the temperature, ΔU_i is the change in the potential energy of creating a particle of type i, Λ_i is the de Broglie wavelength, and ξ is a random number generated uniformly in (0, 1). If accepted, the ion inserted into the control volume is given a velocity from the Gaussian distribution [37] at the temperature at which the MD simulation is performed. A deletion attempt in the control volume is successful if

TABLE I. Parameters for the Lennard-Jones potential $U(r)$ $=C_{12}/r^{12}-C_6/r^6$.

Interaction	C_6 (kJ nm^6 mol^{-1})	C_{12} (kJ nm^{12} mol^{-1})	σ (nm)
O-O	0.2634×10^{-2}	0.2667×10^{-5}	0.317
O-C	0.6254×10^{-2}	0.7752×10^{-5}	0.328
O-Cl	0.6011×10^{-2}	0.1678×10^{-4}	0.375
O-K	0.2459×10^{-2}	0.2897×10^{-5}	0.325
Cl-Cl	0.1380×10^{-1}	0.1069×10^{-3}	0.445
Cl-C	0.1190×10^{-1}	0.3501×10^{-4}	0.3785
Cl-K	0.5588×10^{-2}	0.1866×10^{-4}	0.387
K-K	0.2286×10^{-2}	0.3123×10^{-5}	0.333
K-C	0.5808×10^{-2}	0.8336×10^{-5}	0.336

$$N_i(c)\exp\left[-\beta\mu_i(c)-\ln\frac{V(c)}{\Lambda_i^3}-\beta\Delta U_i\right]\geqslant\xi. \quad (18)$$

In order to verify that the chemical potential in the control volume is maintained, we also calculated the chemical potential of each ionic species in the control volumes during the DCV-GCMD simulation using the Widom's particle insertion method [35,38]. In this method the "test" atoms (ions) are inserted at random positions into the control volume at regular intervals. These inserted "test" ions are assumed to have no influence on the existing ions and water molecules present in the system. If ΔU_i denotes the energy of the "test" ion i with respect to N atoms present in the control volume, the chemical potential of that ionic species μ' in the control volume is given by

$$\beta\mu'=\ln\left(\frac{N_i(c)\sigma^3}{V(c)}\right)-\ln\langle\exp(-\beta\Delta U_i)\rangle, \quad (19)$$

where $\langle\cdots\rangle$ denotes the grand canonical average over the test atoms (ions) of type i in the control volume and σ is the LJ ion-ion distance parameter. The average is calculated over statistical data from randomly inserted test particles of ionic species i into the control volume.

IV. SIMULATION DETAILS

A snapshot of the nanochannel-bath system for self-consistent DCV-GCMD simulation is shown in Fig. 2. The time step used in the MD simulation was 2 fs. Periodic boundary conditions are applied in the y and z directions, but are omitted in the x direction. Walls on extremes of the nanochannel-bath consists of LJ atoms with the parameters of carbon obtained from the GROMOS force field. The entire system between the confining walls was filled with an electrolyte solution of 0.5 *M* KCl. It is assumed that water concentration in the baths does not change significantly with applied electric fields, so it is not monitored during the DCV-GCMD simulation. However, if the water concentration needs to be maintained, umbrella sampling approaches can be used [39]. The channel wall is single layered, with LJ parameters of carbon (Table I). These channel wall atoms are fixed to their original lattice positions, with lateral dimensions of 1.5 nm×4.1 nm. K^+ and Cl^- ions were modeled as

TABLE II. The different nanochannel geometry cases studied, along with the voltages applied on them using SCMD.

Channel length (nm)	Channel height (nm)	Channel width (nm)	Voltage applied (V)
1.5	0.5	2, 3.5	0.9
1.5	1	2, 3.5	0.9
1.5	1.5	2, 3.5	0.9
1.5	4	2, 3.5	0.9

charged LJ atoms with LJ parameters taken from Lynden-Bell and Rasaiah [16,40] (see Table I). Water was modeled using the simple point charge-extended (SPC/E) model. A LINCS algorithm [41] was used to maintain the water geometry specified by the SPC/E model. Electrostatic interactions were calculated by using PME [25] and removing the periodicity in the x direction using the implementation of Yeh and Berkowitz [26]. Fourier grid spacing of the Ewald calculation was 0.125 nm. The real-space cutoff for the electrostatic and LJ calculations was 1 nm. A Berendsen thermostat [42] with a time constant of 0.1 ps was used to maintain the temperature of the fluid at 300 K. The LJ parameters for the "ghost" atoms are listed in Table I. The MD simulation is set up with an initial input of the total number of atoms ("ghost" atoms+ions+water molecules), which does not change during the simulation.

The electrodes are placed 1.5 nm away on either side of the nanochannel in the x direction. The applied external electric field was treated using the two different approaches. In self-consistent DCV-GCMD simulations, 0.9 and 0 V were applied on the left and right electrodes, respectively. In the uniform field MD simulation, a uniform potential drop of 0.2 V/nm (obtained assuming 0.9 V drops uniformly) was applied across the length of 4.5 nm from the end of one bath to the other. When a potential is applied on the electrodes, the channel length, channel height, and channel width are the important dimensions that affect the electric field distribution in and around the nanochannel. From the Poisson solution, the higher the channel height to the channel width ratio, the higher is the potential drop in the nanochannel compared to the potential drop in the bath. The dimensions of the nanochannel and baths along with the applied potential and field when using SCMD and uniform field MD simulations are given in Table II. The four nanochannel models studied have channel heights of 0.5 nm, 1 nm, 1.5 nm, and 4 nm. The nanochannel has a length of 1.5 nm. Two different channel widths of 3.5 nm and 2 nm are considered in this study. The x and y directions of the simulation box have dimensions of 6 nm and 4.1 nm, respectively. The box length in the z direction varies depending on the channel height and channel width. The length of the control volume in each bath is 0.75 nm and the length of the "ghost" reservoir is 1.5 nm in the x direction. The two control volumes are maintained at a concentration of 0.5 M KCl. With an applied electric field of 0.2 V/nm in the x direction, the chemical potentials of K$^+$ and Cl$^-$ ions were calculated using Widom's test particle method on four test NVT MD simulations with 0.5 M KCl in a 4 nm $\times$ 4 nm $\times$ 4 nm box. The calculated chemical poten-
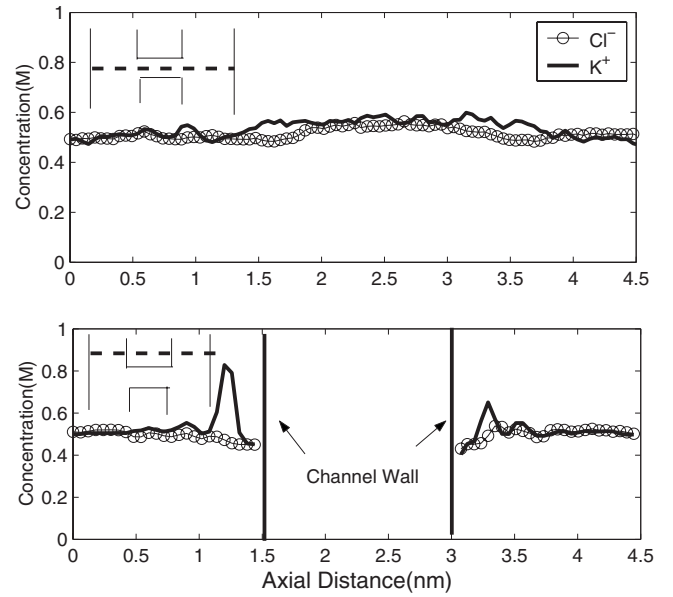

FIG. 3. Concentration profiles (axial) of the potassium (K$^+$) and chloride (Cl$^-$) ions at the center of the channel (top) and at half the channel height (bottom) with an applied field of 0.2 V/nm.

tials for the K$^+$ and Cl$^-$ ions, input to the two control volumes in DCV-GCMD simulations studied hereafter, are found to be -2.45 and -1.87 kJ mol^{-1}, respectively.

V. VERIFICATION OF DCV-GCMD

In DCV-GCMD simulations, the stochastic insertion or deletion step to the MD step ratio ($n_{trial}:n_{MD}$) is important in maintaining the ion density and chemical potential in the control volume. After every n_{MD} MD steps, the system is frozen in time to perform n_{trial} insertion or deletion trials. n_{trial} needs to be as small as possible to reduce the computational time, while being large enough to maintain the density of ions in the control volumes. Incorrect n_{trial} will lead to incorrect ionic densities of K$^+$ and Cl$^-$ ions in the control volumes. If the n_{MD} parameter is too high, then the control volume could lose more ions compared to the ions that are inserted from the stochastic step, thus steadily decreasing the concentration of the ions in the control volume or vice versa. For the nanochannel-bath example considered here, the concentrations of K$^+$ and Cl$^-$ ions in both the control volumes are maintained using a small value of n_{trial}, since the number of K$^+$ and Cl$^-$ ions added or removed from the control volume is small.

Verification of the DCV-GCMD simulation was carried out for a 3.5-nm-wide channel with a channel height of 0.5 nm using a uniform external electric field of 0.2 V/nm in the x direction. n_{trial} values ranging from 20 to 200 were tested to obtain an optimum value of 50 to maintain a 0.5M KCl concentration in the control volume. To select n_{MD}, the number of K$^+$ and Cl$^-$ ions moving in and out of the control volume for n_{MD} of 50, 100, and 200 was estimated. The optimum value of $n_{MD}=100$ was chosen because with the applied electric field of 0.2 V/nm, the number of ions moving in or out of the control volume in 0.02 ps is on an aver-
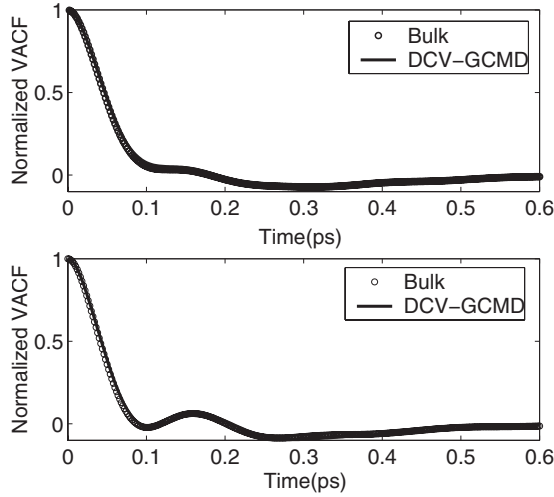
FIG. 4. Equilibrium velocity autocorrelation function (VACF) calculations of K^+ (top) and Cl^- (bottom) ions in the reservoirs of the nanochannel-bath system maintained at 0.5 M KCl. The bulk values and DCV-GCMD results are comparable.

age 0.7, which corresponds to a $0.08M$ ion concentration fluctuation in the control volume. Thus, the n_{trial} to n_{MD} ratio was kept at 50:100 for all channel dimensions studied in this paper. The concentration profiles for the K^+ and Cl^- ions along the axial direction were calculated using the "binning" method [43]. Figure 3 shows the density profiles for the K^+ and Cl^- ions along the centerline in the x direction ($z=L_z/2$, where $L_z=4.5$ nm is the box length in the z direction). The concentration profiles along the axial direction at half the channel height have also been plotted. The concentrations of the K^+ and Cl^- ions in the two control volumes are maintained at 0.5 M, indicating that the chemical potential used for K^+ and Cl^- ions is reasonably accurate.

To ensure that the dynamics of the DCV-GCMD simulation was not affected by the stochastic step, the velocity autocorrelation function (VACF), which is a measure of the time an atom takes to loose its thermally gained velocity [44], was calculated using the expression

$$C_{v;k}(t) = \frac{\langle v_k(t)v_k(0)\rangle}{\langle v_k(0)v_k(0)\rangle}, \quad (20)$$

where $v_k(t)$ is the velocity of ion k at time t. An equilibrium DCV-GCMD simulation with no external electric field was carried out with the same setup as described above. The VACF was calculated in the reservoir region 0.4 nm away from the membrane. After equilibration for 1 ns, statistics were collected every 0.1 ps for 2 ns. The VACF for K^+ and Cl^- ions is found to be comparable to that given in [45] for a 0.88-M bulk KCl solution, as shown in Fig. 4. The translational self-diffusion coefficient D_k of an ion k can then be calculated from the time integral of the VACF in the Green-Kubo integrand [46], given by

$$D_k = \frac{k_B T}{m_k}\int_0^\infty C_{v;k}(t)dt, \quad (21)$$

where k_B is the Boltzmann constant and m_k is the mass of ion k. D_k calculated in the DCV-GCMD simulation for K^+ and Cl^- ions are found to be 1.79×10^{-5} cm^2 s^{-1} and 1.53×10^{-5} cm^2 s^{-1}, respectively. The bulk diffusion coefficient values for K^+ (1.82×10^{-5} cm^2 s^{-1}) and Cl^- (1.55×10^{-5} cm^2 s^{-1}) ions [46] are comparable to those obtained from the reservoirs in the DCV-GCMD simulation. The reasonable D_k values and constant concentrations maintained over the DCV-GCMD simulation implies that the dynamics of the DCV-GCMD simulation is preserved.

VI. RESULTS

In this section, we present several examples comparing the SCMD simulations, uniform applied electric field MD simulations, and classical continuum theory simulations. The classical continuum theory for electric-field-mediated ion transport is given by the Poisson equation (1) and the Nernst-Planck equation

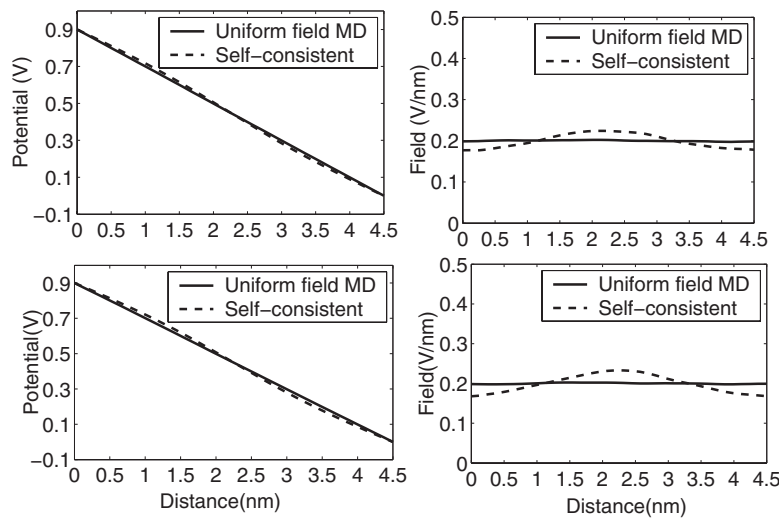$$\nabla \cdot J_i = 0 \quad \text{in } \Omega, \quad (22)$$

FIG. 5. Self-consistent vs uniform field MD calculations: potential (left) and electric field (right) calculations in the axial direction along the center of the 3.5-nm-wide nanochannel; channel height=0.5 nm (top), 1.5 nm (bottom).
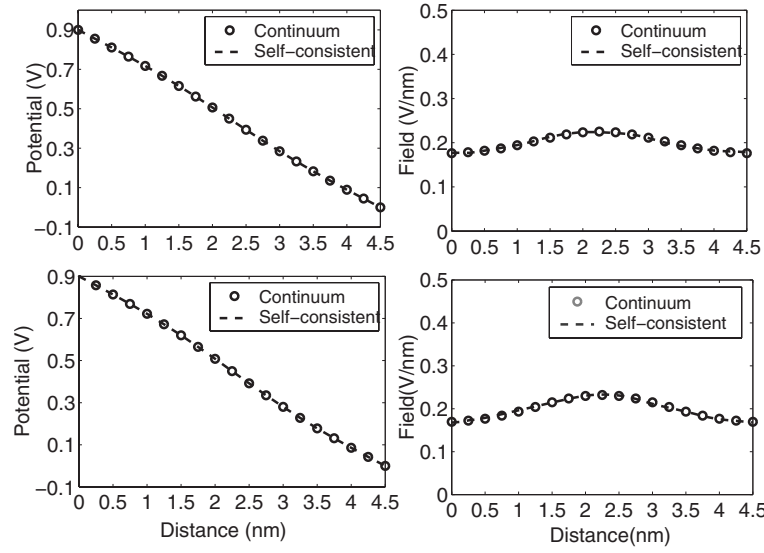
FIG. 6. Self-consistent vs continuum calculations: potential (left) and electric field (right) calculations in the axial direction along the center of the 3.5-nm-wide nanochannel; channel height=0.5 nm (top), 1.5 nm (bottom).

$$J_i = -D_i \nabla c_i - \mu_i z_i F c_i \nabla \phi \quad \text{in } \Omega, \quad i = 1, \dots, N. \quad (23)$$

In the above equations, ϕ is the electrostatic potential obtained by solving Eq. (1), J_i is the flux of ionic species i, c_i is the concentration of the ith ionic species, z_i is the valency of the species i, D_i and μ_i are the diffusion coefficient and mobility of species i, respectively, and N is the total number of species. For continuum calculations, the relative permittivity of water, ϵ_r, in Eq. (1), is assumed to be 80, its bulk value. Boundary conditions to solve Eq. (1) are as given in Eqs. (3–6). The boundary conditions to solve Eqs. (22) and (23) are zero flux on Γ_i, $i=3,\dots,8$, and Dirichlet boundary conditions, $c_i = 0.5\ M$, on Γ_1 and Γ_2.

A. Comparison of the electrical potential and field

Electrical potential and electric field calculations in MD simulations of nanochannels are important as they affect the water and ion transport, ion selectivity, and current-voltage (I-V) characteristics in the channel. The electrical potential ϕ (ϕ is the total potential including the particular solution and the homogeneous solution) is calculated as described in Sec. II. Figure 5 shows the SCMD and uniform field MD results for the electrical potential and the x component of the electric field in the axial direction (x direction) along the centerline of the 3.5 nm nanochannel for channel heights of 0.5 and 1.5 nm, respectively. For the potential and electric field profiles obtained in the large channel height case of 1.5 nm,
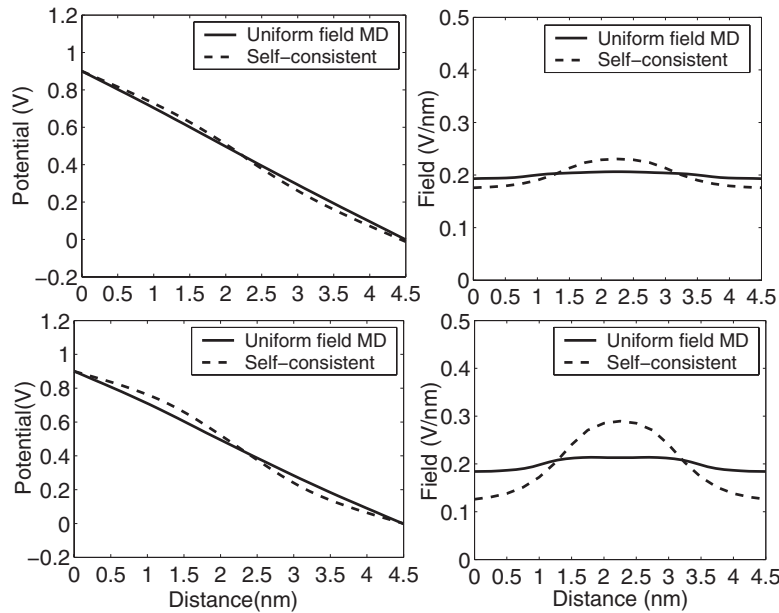

FIG. 7. Self-consistent vs uniform field MD calculations for a 2-nm-wide channel: potential (left) and electric field (right) calculations in the axial direction along the center of the nanochannel system; channel height=0.5 nm (top), 1.5 nm (bottom).
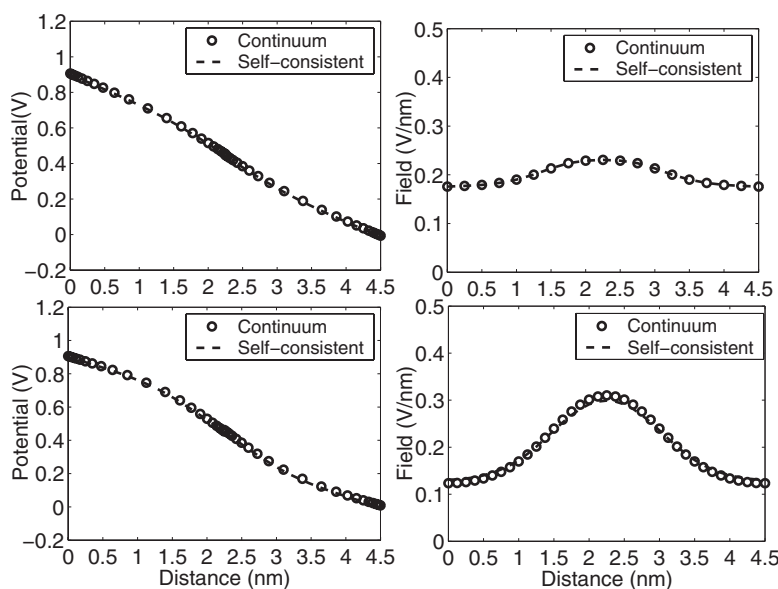
FIG. 8. Self-consistent vs continuum calculations for a 2-nm-wide channel: potential (left) and electric field (right) calculations in the axial direction along the center of the nanochannel system; channel height=0.5 nm (top), 1.5 nm (bottom).

SCMD simulation shows a higher potential drop in the channel region and a corresponding reduction in the potential drop in the reservoir region when compared to the 0.5-nm-channel-height case. In the uniform field MD formulation, the potential drop is lower across the nanochannel compared to SCMD. Note that in the uniform field MD formulation, though the applied electric field is constant, the total electric field is not necessarily constant in the entire nanochannel-bath system due to the electric field from the particular solution. In the case of 1.5 nm channel height, a difference of 8% in the electric field along the channel centerline is observed in the middle of the channel between the two formulations. This difference in the electric field can result in different ion migration rates and transport properties in the nanochannel system from SCMD and uniform field MD simulations. SCMD results for the electrical potential and electric field are also compared with the results from the classical theory [see Eq. (22)]. We do not expect the results from the classical theory to match with SCMD in the entire system, but along the centerline of the channel, the classical theory can be a good approximation because of the bulklike nature of the electrolyte along the centerline. Figure 6 compares the electrical potential and field obtained from continuum theory with SCMD for nanochannels with channel heights of 0.5 and 1.5 nm. The potential profiles at the centerline region along the x direction are in good agreement.

Figure 7 shows the electrical potential and field along the centerline of the channel for a 2-nm-wide channel with channel heights of 0.5 and 1.5 nm, respectively. While the electrical potential and field along the centerline region from SCMD and uniform field MD simulations are comparable in the 0.5-nm-channel-height case, the electric field in the middle of the channel is 25% higher in SCMD for the 1.5-nm-channel-height case. Figure 8 compares the electrical potential and the electric field obtained from continuum theory with SCMD for nanochannel-bath systems with channel heights of 0.5 and 1.5 nm. The results compare well ex-

cept for the 1.5-nm-channel-height case where there is a small deviation in the electric field between SCMD and continuum calculations. Though the electrical potential and field obtained from the continuum theory are in good agreement with SCMD results in the centerline region, the electrical potential near the interfacial region from the continuum theory can be in significant error when compared with the SCMD results. For example, the electrical potentials along the center of the nanochannel in the z direction for the 3.5- and 2-nm-wide channels with a channel height of 1.5 nm are shown in Figs. 9 and 10, respectively. Clearly, near the channel wall the deviation between the two theories is quite significant. The continuum theory predicts a constant potential which is not correct. The continuum theory prediction deviates from the SCMD prediction due to the layering of water and ions and finite-size effects of ions which are not included in the continuum theory.
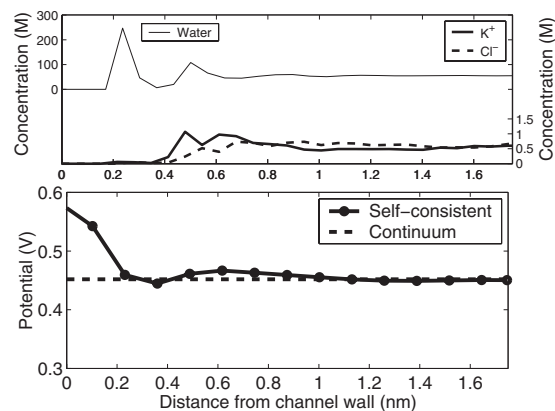

FIG. 9. Concentration profile (top) and electrostatic potential (bottom) in the midsection (parallel to channel wall normal) of the 3.5-nm-channel-width case with a channel height of 1.5 nm. The potential is plotted until the center of the channel.
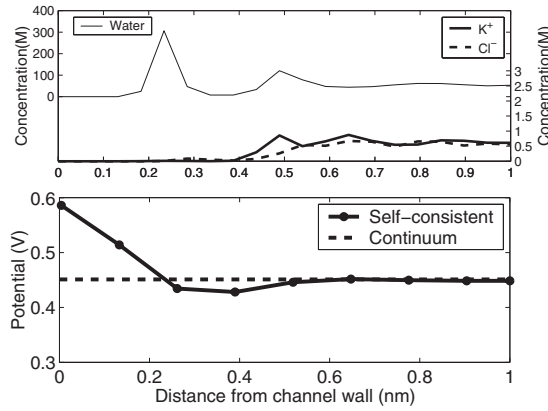
FIG. 10. Concentration profile (top) and electrostatic potential (bottom) plotted for the midsection (parallel to channel wall normal) of the 2-nm-channel-width case with a channel height of 1.5 nm. The potential is plotted until the center of the channel.

B. Translocation times and ionic fluxes

To understand the effect of the electric field on ion transport properties, we computed the translocation times of ions using the uniform field MD and SCMD approaches. The translocation time of an ion is defined as the time it takes an ion to travel from one end of the nanochannel to the other end. The calculated translocation times for the channels with widths of 3.5 nm and 2 nm are given in Table III. A number of observations can be made from the data presented in the table. First, for the same channel width, as the channel height increases, the translocation times of ions decrease in the SCMD approach. This is due to the corresponding increase in the average electric field observed inside the channel region, as described in the previous section. However, in the case of uniform field MD, the translocation times do not vary significantly as there is no significant change in the average electric field with increasing channel height. Second, for a smaller channel height to width ratio, the translocation times of ions are found to be similar using both SCMD and uniform field MD simulations. Therefore, we can conclude that for smaller channel height to width ratios, the uniform field MD treatment can still provide accurate results. Third, for the same channel height, as the channel width decreases, the translocation times of ions increase. This is because the mobility of an ion decreases as the channel width decreases due to confinement. For example, the average mobility values of K^+ and Cl^- ions in the channel region for the
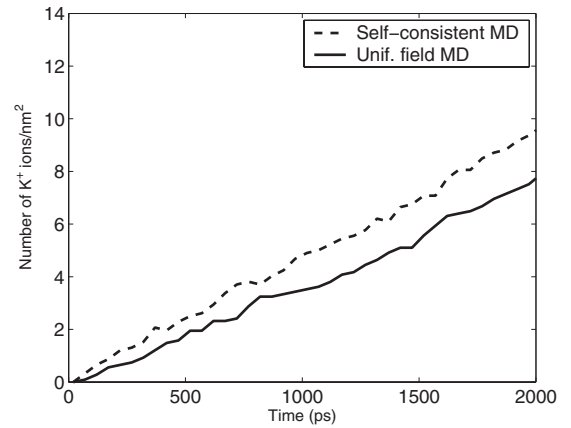

FIG. 11. Comparison of the accumulated K^+ ions per unit area [number/(nm^2)] with time in the 3.5-nm-channel-width case for a channel height of 4 nm.

2-nm-wide channels are found to be 5.1×10^{-4} cm^2 V^{-1} s^{-1} and 4.18×10^{-4} cm^2 V^{-1} s^{-1}, respectively, while the corresponding mobility values in the channel region for the 3.5-nm-wide channels are 5.84×10^{-4} cm^2 V^{-1} s^{-1} and 4.5×10^{-4} cm^2 V^{-1} s^{-1}.

Next, we compute the ionic fluxes to investigate the dependence of the ionic flux on the electric field. The total number of ions passing through the nanochannel was measured and accumulated over time to obtain the ionic flux. The statistical data were collected every 0.1 ps from the MD simulations after a 2 ns equilibration time. The average accumulation of K^+ ions over a 2 ns time scale for the 3.5-nm-wide channel with channel heights of 0.5 nm and 4 nm was calculated. The K^+ ionic flux variation is observed to be similar from both SCMD and uniform field MD simulations for the 0.5-nm-channel-height case. However, when the channel height is 4 nm, the accumulated K^+ ionic flux calculated from SCMD is 4.66/(nm^2 ns) while that observed in uniform field MD is 3.74/(nm^2 ns) (see Fig. 11). Therefore, in SCMD, the ions go through the nanochannel faster, leading to a higher flux, which is not captured in the uniform field MD simulation. Similar observations were made for the Cl^- ionic flux. We also studied the effect of the electric field on the ionic fluxes in the 2-nm-wide channel. The observations were again consistent; i.e., the ionic fluxes from SCMD and uniform field MD simulations are comparable for the 0.5-nm-channel-height case. For the 4-nm-channel-height case, uniform field MD underestimates the K^+ ionic flux by

TABLE III. Translocation times of ions in picoseconds, calculated from the self-consistent and uniform field MD treatments.

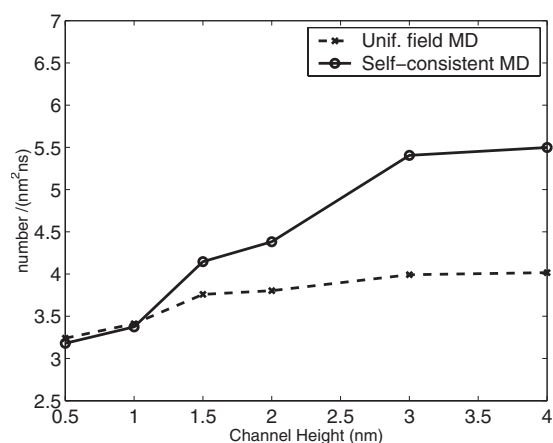| Channel height	Species	Channel width=3.5 nm		Channel width=2 nm	
		Self-consistent	Uniform field	Self-consistent	Uniform field
0.5 nm	K^+	164	171	190	193
0.5 nm	Cl^-	202	210	231	236
1.5 nm	K^+	147	168	158	184
1.5 nm	Cl^-	185	207	197	223

FIG. 12. Comparison of the accumulated total ion fluxes [number/(nm^2 ns)] in the 2-nm-channel-width case with increasing channel height.

25%. The variation of the total ionic flux (including both the K^+ and Cl^- ions) with channel height is shown in Fig. 12. The results from both SCMD and uniform field MD are shown for comparison. For increasing channel heights (i.e., as the channel height to width ratio increases), the results from uniform field MD deviate significantly from SCMD, signifying the effect of the geometry and the need for an accurate treatment of the applied electric field in MD simulations.

C. Channel selectivity

To understand the effect of the applied electric field on the channel selectivity, SCMD and uniform field MD simulations were compared for a 1-nm-wide channel with a channel height of 1.5 nm. The electrode potentials were kept the same as in the previous examples. It is found that during a 2 ns simulation time, the K^+ ions go through the channel in

SCMD simulations, while in the uniform field MD simulations no ion gets through the nanochannel. Figure 13 shows the trajectory of a K^+ ion transport in the SCMD and uniform field MD simulations in 2 ns. This dramatic difference in the transport of ions observed between the two simulations implies that the selectivity of a nanochannel can be accurately studied only with a proper treatment of the applied electric field in molecular dynamics simulations.

VII. CONCLUSION

A self-consistent treatment of an externally applied electric field in molecular dynamics simulations for a nanochannel-bath system has been presented. The concentration of the ions in the reservoir is maintained by using the DCV-GCMD technique extended for electrolytic solutions. The SCMD approach has been compared with the uniform field MD approach to understand the limitations of the uniform field treatment. By comparing results for different channels widths and channel heights, it was found that as the ratio of the channel height to width increases, the electrostatic potential and the electric field obtained with the SCMD can be quite different from the uniform field approach. Furthermore, the translocation times of ions and ionic fluxes have been found to be quite different between SCMD and uniform field approaches. Finally, it was also observed that for a 1-nm-wide channel, a K^+ ion does not permeate the nanochannel with a uniform field approximation, but the K^+ ion was found to permeate the nanochannel with a self-consistent treatment of the applied electric field.
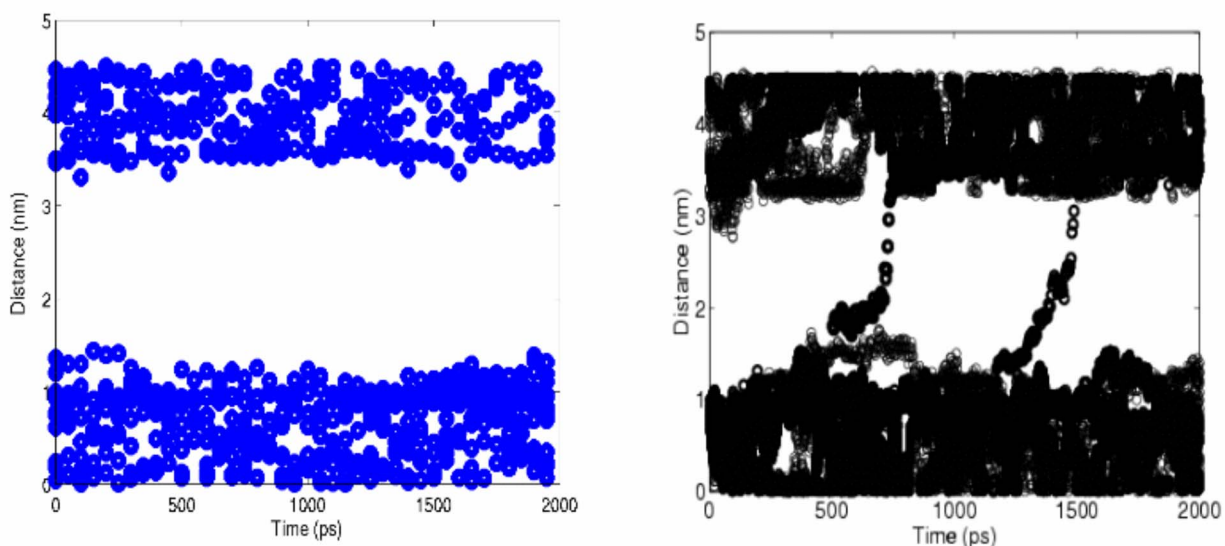
FIG. 13. (Color online) Trajectory of K^+ ions in the uniform field MD (left) and SCMD (right) simulations of a 1-nm wide channel.

APPENDIX

Algorithm: The DCV-GCMD approach

1:    Input: N interacting atoms (ions and water molecules), force field, time step Δt, number of MD steps, n_{MD}, after which a stochastic step is to be performed, and μ_i, the chemical potential of species i.

2:    Set n_{trial}, the number of insertion and deletion trials and total MD steps, n_{tot}.

3:    Start the DCV-GCMD simulation. Step $n=0$, time $t=0$.

4:    *Repeat*

5:      Set $n=n+1$

6:      *If* n is a multiple of n_{MD}, *then*

7:        Freeze the MD simulation in time.

8:        Perform n_{trial} insertion or deletion stochastic steps of ions in the two control volumes.

9:        *If* insertion of an ion is *accepted*, a ghost; atom from the ghost reservoir is taken and inserted into the control volume with appropriate LJ and charge parameters.

10:      *If* deletion of an ion is *accepted*, the ion from the control volume is placed in the ghost reservoir with ghost atom LJ parameters and no charge.

11:      Calculate the change in potential for trial insertion and deletion of the ion in the control volume ΔU.

12:      Accumulate the Boltzmann factor $\exp(-\beta\Delta U)$, for use in the Widom's particle method [see Eq. (19)].

13:      *End if*

14:      Perform MD step for time t.

15:      $t=t+\Delta t$

16:    *Until* $n>n_{tot}$.

[1] G. E. Karniadakis, A. Beskok, and N. R. Aluru, *Microflows and Nanoflows: Fundamentals and Simulation* (Springer, New York, 2005).

[2] B. Hille, *Ion Channels of Excitable Membranes* (Sinauer Associates, Sunderland, 2001).

[3] P. Buhlmann, H. Aoki, K. P. Xiao, S. Amemiya, K. Tohda, and Y. Umezawa, Electroanalysis **10**, 1149 (1998).

[4] T.-C. Kuo, L. A. Sloan, J. V. Sweedler, and P. W. Bohn, Langmuir **17**, 6298 (2001).

[5] D. Levitt, Biophys. J. **52**, 455 (1987).

[6] M. Sancho and G. Martinez, Biophys. J. **60**, 81 (1991).

[7] A. E. Cardena, R. D. Coalson, and M. G. Kurnikova, Biophys. J. **79**, 80 (2000).

[8] Z. Schuss, B. Nadler, and R. S. Eisenberg, Phys. Rev. E **64**, 036116 (2001).

[9] S. H. Chung, T. W. Allen, M. Hoyles, and S. Kuyucak, Biophys. J. **75**, 793 (1999).

[10] B. Corry, S. Kuyucak, and S. H. Chung, Biophys. J. **78**, 2364 (2000).

[11] K. P. Travis and K. E. Gubbins, J. Chem. Phys. **112**, 1984 (2000).

[12] L. Cheng, P. Fenter, K. L. Nagy, M. L. Schlegel, and N. C. Sturchio, Phys. Rev. Lett. **87**, 156103 (2001).

[13] M. E. Tuckerman and G. J. Martyna, J. Phys. Chem. **104**, 159 (2000).

[14] H. Shrivastava and M. S. Sansom, Biophys. J. **78**, 557 (2000).

[15] J. Hu, S. Goldman, C. G. Gray, and H. R. Guy, Mol. Phys. **98**, 535 (2000).

[16] R. M. Lynden-Bell and J. C. Rasaiah, J. Chem. Phys. **105**, 9266 (1996).

[17] S. C. Li, M. Hoyles, S. Kuyucak, and S.-H. Chung, Biophys. J. **74**, 37 (1998).

[18] P. S. Crozier, D. Henderson, R. L. Rowley, and D. D. Busath, Biophys. J. **81**, 3077 (2001).

[19] V. Ramakrishnan, D. Henderson, and D. D. Busath, Biochim. Biophys. Acta **1664**, 1 (2004).

[20] V. Ballenegger and J. P. Hansen, J. Chem. Phys. **122**, 114711 (2005).

[21] H. A. Stern, J. Chem. Phys. **118**, 3401 (2003).

[22] A. N. Tikhonov and A. A. Samarskii, *Equations of Mathematical Physics* (Dover, New York, 1990).

[23] T. Tsang, *Classical Electrodynamics* (World Scientific, Englewood Cliffs, NJ. 1997).

[24] L. Greengard and V. Rokhlin, J. Comput. Phys. **73**, 325 (1987).

[25] T. Darden, D. York, and L. Pedersen, J. Chem. Phys. **98**, 10089 (1993).

[26] I. Yeh and M. L. Berkowitz, J. Chem. Phys. **111**, 3155 (1999).

[27] M. T. Heath, *Scientific Computing* (McGraw-Hill, New York, 2002).

[28] G. University, GROMACS User Manual 3.1.4, Nijenborgh 4,9747 AG Groningen, The Netherlands, http://www.gromacs.org

[29] J. Zheng, E. M. Lennon, H.-K. Tsao, Y.-J. Sheng, and S. Jiang, J. Chem. Phys. **122**, 214702 (2005).

[30] P. Attard, J. Chem. Phys. **121**, 7076 (2004).

[31] Q. Zhang, J. Chem. Phys. **117**, 808 (2002).

[32] S. Boinepalli and P. Attard, J. Chem. Phys. **119**, 12769 (2003).

[33] G. S. Heffelfinger and F. van Swol, J. Chem. Phys. **100**, 7548 (1994).

[34] J. M. Hammersley and D. C. Handscomb, *Monte Carlo Methods* (Wiley, New York, 1964).

[35] K. Ding and J. P. Valleau, J. Chem. Phys. **98**, 3306 (1994).

[36] E. Lindahl, B. Hess, and D. van der Spoel, J. Mol. Model. **7**, 306 (2001).

[37] M. Lsal, J. K. Brennan, W. R. Smith, and F. R. Siperstein, J. Chem. Phys. **121**, 4901 (2004).

[38] J. R. Henderson, Mol. Phys. **50**, 741 (1983).

[39] T. Kuznetsova and B. R. Kvamme, Mol. Phys. **97**, 423 (1999).

[40] D. E. Smith and L. X. Dang, J. Chem. Phys. **100**, 3757 (1994).

[41] B. Hess, H. Bekker, H. Berendsen, and J. Fraaije, J. Comput. Chem. **18**, 1463 (1997).

[42] H. J. C. Berendsen, J. P. M. Postma, W. F. van Gunsteren, A. DiNola, and J. R. Haak, J. Chem. Phys. **81**, 3684 (1984).

[43] M. P. Allen and D. J. Tildeley, *Computer Simulation of Liquids* (Kluwer, Dordrecht, 1993).

[44] D. Frenkel and B. Smith, *Understanding Molecular Simulation* (Academic Press, San Diego, 2001).

[45] S. Chowdhuri and A. Chandra, J. Chem. Phys. **115**, 3732 (2001).

[46] D. J. Evans and J. P. Morris, *Statistical Mechanics of Nonequilibrium Liquids* (Academic Press, London, 1990).